Transmission Electron Microscopy of Welded Cb-Microalloyed Steel

The effects of resistance spot welding and GMA welding on the columbium precipitates in a microalloyed steel are investigated

BY P. L. MANGONON

ABSTRACT. Transmission electron microscopy (TEM) of weld microstructures was conducted in 0.100 in. (2.5 mm) thick 50 ksi (348 MPa) minimum yield strength Cb-bearing controlled rolled HSLA steel, as well as in 0.100 in. (2.5 mm) thick SAE 1005 steel. The processes used were resistance spot welding and GMAW at heat inputs from 4.6 to 6.4 Joules/in. (0.8 to 0.25 Joules/mm).

In spot welding, the influence of hold-time after welding on the microstructures and reprecipitation of columbium carbonitride was investigated. In GMA welding, modifications in the columbium precipitates were observed with changes in weld heat input. These modifications are similar to those observed in submerged arc welded plates reported in the literature; they did not impair the notch toughness properties of the GMAW steel as measured by a specially designed tension-impact test.

Introduction

Small additions of columbium (Cb) impart beneficial effects to the structures and properties of micro-alloyed HSLA steels. The effects are attained by controlled processing and may include:

1. Austenite grain refinement during soaking.
2. Keeping the austenite in the unrecrystallized condition during hot-rolling to produce very fine ferrite grains during transformation.
3. Increasing the hardenability when in solution in austenite.
4. Strengthening the ferrite by precipitating as very fine columbium-carbonitride particles.

It is generally agreed that the carbonitride particles forming in austenite contribute insignificantly to the final strength. To be effective strengthener, the size of particles needs to be on the order of 2-5 nm (7.9 to 19.7 × 10^{-9} in.) when precipitating in ferrite. For strip products, this size can be achieved by controlling the coiling temperature.

The optimum microstructures and carbonitride particles produced after controlled processing are obliterated during welding. Depending upon welding conditions the carbonitride particles may dissolve or may undergo high temperature modifications. In a study to determine the influence of columbium and titanium in submerged arc welded carbon-manganese plate steels (Refs. 1, 2), plate-like eutectic-type carbide precipitates were observed at primary grain or dendritic cell boundaries in the weld. These plate-like carbides are apparently different from those carbides which dissolve during soaking at about 1150-1200°C (2102-2192°F).

Rather than dissolve, the plate-like carbides continued to precipitate at the boundaries of primary grains from 1300°C (2372°F) to the solidus temperature. These high-temperature carbides were also observed in heavy forgings and heavy castings of a steel containing columbium (Ref. 3). The plate carbides were considered responsible for the intergranular "rock-candy" brittle fractures in heavy castings.

Columbium oxysulfides were also observed to form eutectic intergranular films in the HAZ and very close to the fusion line (Ref. 2). These sulfides appeared to have lower melting points than that of MnS and may have resulted in hot cracking and reduced ductility. In another study (Ref. 4), eutectic linear columbium carbonitrides and eutectic sulfonitrides formed between 1350-1500°C (2462-2732°F). The latter study simulated the welding cycle by annealing specimens between 1200°C (2192°F) and the melting point, followed by slow or rapid cooling. These precipitate variations prompted the IIW to limit the columbium content to less than 0.05 wt-% as a precautionary measure.

The columbium precipitates were identified by electron microscopy (Refs. 1-4) after carbon extractions from fractured surfaces. All were observed in replicas made from either heavy forgings and castings or welded plates thicker than 15 mm (0.59 in.). The present paper reports on the observance of similar precipitates by TEM of thin foils from the 2.5 mm (0.100 in.) GMA welded specimens. The substructures produced after spot and GMA welding are also described for both a columbium-bearing and a plain carbon steel.

Materials and Procedures

The materials were taken from commercially produced coiled hot-strip 2.54 mm (0.100 in.) thick Hi-Form 50 (Inland Steel's 50 ksi or 345 MPa minimum yield strength steel and described as HF 50 steel in the balance of this paper); SAE 1005 steels were also used. The compositions and tensile properties of these steels are shown in Tables 1 and 2, respectively. The HF 50 steel was primarily developed for automotive application, and its processing, structures, and properties have been described elsewhere

P. L. MANGONON is with the Department of Mechanical Engineering, Florida Institute of Technology, Melbourne, Florida.

Table 1—Chemical Compositions of Steels, Wt-%

	0.106 in. thick SAE 1005 steel	0.100 in. thick HF 50 steel
C	0.04	0.06
Mn	0.33	0.33
P	0.008	0.008
S	0.017	0.029
Si	0.003	0.081
Cu	0.06	—
Cb	—	0.036
Al	0.005	0.046
N	0.005	0.006
Fe	Bal.	Bal.

(Ref. 5).

The spot- and GMA-welded properties of HF 50 were also the subject of another presentation (Ref. 6). The electron microscopy that will be described here was carried out on the materials used in that presentation. The resistance spot welding conditions are listed in Table 3 where the principal variable studied was hold time.

For GMA welding, two welding wires were used; their compositions are shown in Table 4. Welding procedure consisted of spacing the square edges of the light-gage steels about 1.125 mm (0.045 in.) apart (the diameter of the weld wires) in a flat position with no backing material and no preheat. The weld joint was made using a stringer bead technique to obtain complete joint penetration in one pass. The welding conditions are shown in Table 5.

Thin foils for transmission electron microscopy (TEM) were prepared from specimens containing the original hot-rolled surfaces; the welded joints, shown in Fig. 1, are situated in the middle of the surfaces. These were ground to remove equal amounts from both sides and polished with one-micron grit diamond to about 0.5 mm (0.020 in.), then chemically polished to about 0.05 mm (0.002 in.), and—finally—electropolished to obtain the foils. During electropolishing, slight etching occurred to delineate the weld and heat-affected zones where the foils were obtained. The foils were examined with the Philips EM 300 microscope operated at 100 kV.

Table 2—Tensile Properties of Steels

	0.106 in. thick SAE 1005 steel	0.100 in. thick HF 50 steel
Yield strength (0.2% offset), psi	41,000	56,900
Tensile strength, psi	54,200	69,600
Total elongation, %	37	31
Uniform elongation, %	23.5	20

Table 3—Resistance Spot Welding Conditions

Material		Welding current, A	Welding time, Hz	Hold time, Hz	Electrode force, lb	Electrode diameter, in.
HF 50	(1)	15,900	30	50	1800	0.375
(0.100 in.)	(2)	15,900	30	1	1800	0.375
SAE 1005	(1)	10,100	30	50	1600	0.375
(0.100 in.)	(2)	10,100	30	1	1600	0.375

Table 4—Chemical Compositions of 0.045 in. Diameter Welding Wires, Wt-%

	Wire A	Wire B
C	0.10	0.07
Mn	1.19	1.77
P	0.011	0.015
S	0.024	0.012
Si	0.53	0.41
Mo	—	0.42
Fe	Bal.	Bal.

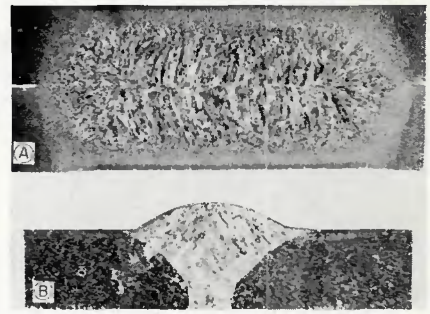

Fig. 1—Weld cross sections: A—resistance spot weld; B—GMA weld. Base metal plate thicknesses are 0.100 in.

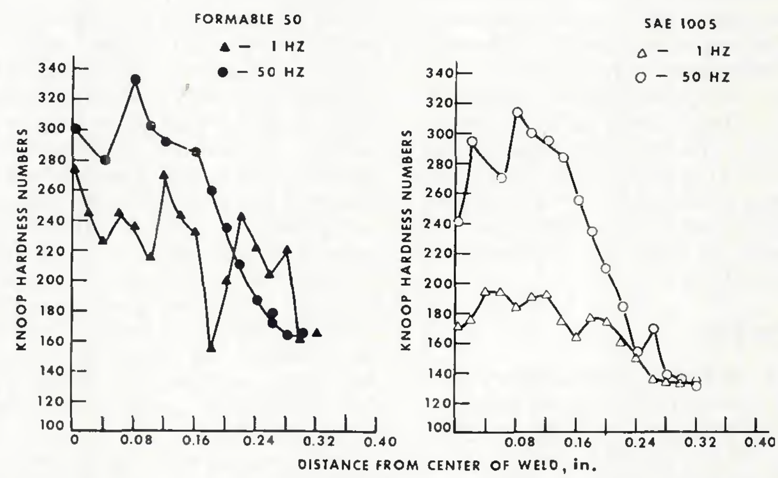

Fig. 2—The effect of one and 50 cycle hold time on the hardness profiles of HF 50 and SAE 1005 steels (distances are in inches)

Table 5—GMA Welding Conditions

Steel	Thickness, in.	Welding wire	Current, A	Arc voltage, V	Welding speed, ipm	Shielding gas	Shielding gas flow rate, cfh	Heat input, J/in.
HF 50	0.100	B	220	26	75	Ar + 1% O_2	35	4550
SAE 1005	0.106	B	260	26	68	Ar + 1% O_2	35	5850
HF 50	0.100	A	240	28	65	CO_2	35	6200
SAE 1005	0.106	A	245	28	64	CO_2	35	6430

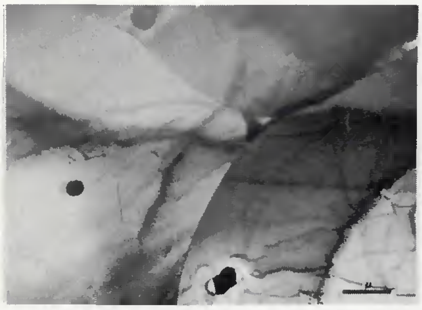

Fig. 3 — Base metal microstructure of SAE 1005 steel

Results and Discussion

Spot Welding

Hardness profiles for the spot welded specimens are portrayed in Fig. 2. One notes that the hardness profiles of the specimens with a hold time of 50 Hz after welding were essentially the same. Since there was no filler material, this result indicates that the strengthening effect of columbium was obliterated at the weld. For the specimens with a hold time of 1 Hz, the columbium steel exhibited significantly higher hardnesses across the weld than the plain carbon steel.

The foregoing results can be explained on the basis of structures developed after welding and after the hold cycles. For comparison, the base metal microstructures are illustrated in Figs. 3 and 4 for the plain carbon and columbium-bearing steels, respectively. The plain carbon steel exhibited relatively low dislocation density with carbides isolated within the grains and also at grain boundaries. In addition to a higher dislocation density, the columbium steel exhibited both degenerate pearlite structure (Fig. 4B) and columbium carbonitride particles (Fig. 4A).

While some of these features might contribute to the strengthening, the significant contribution to the strength in this hot-rolled grade of steel is derived from the ferrite grain-size refinement (Ref. 7). The microstructures obtained after welding and 50 Hz hold time are shown in Figs. 5 and 6, respectively, for the plain-carbon and columbium-bearing steels. The similarity in structures is evident. Both steels exhibited highly dislocated, strained martensitic lath and massive ferrite structures with dissolved and undissolved carbides.

In the martensitic lath structures, the dissolved, cementite carbides reprecipitate at definite orientations within the lath because of auto-tempering, as pointed out by the arrowed lath in Fig. 5A. On the other hand the morphology of the carbides in Fig. 6A suggests these were undissolved because they cross the lath boundaries. Another difference is that the undissolved carbides were generally larger and more rounded than the reprecipitated plate-like carbides in Figs. 5B and 6B.

The larger carbides were from the original base metal microstructures produced during hot-coiling; these became more rounded because of the process of dissolution during welding. Both carbide morphologies are clearly evident in Figs. 5B and 6B, while Figs. 6C and 6D depict bright-field and dark-field images of reprecipitated plate-like carbides. Figure 6C also shows much smaller carbide particles (right upper-half) which are presumably undissolved columbium carbonitrides. The latter are relatively larger and are spaced farther apart than those

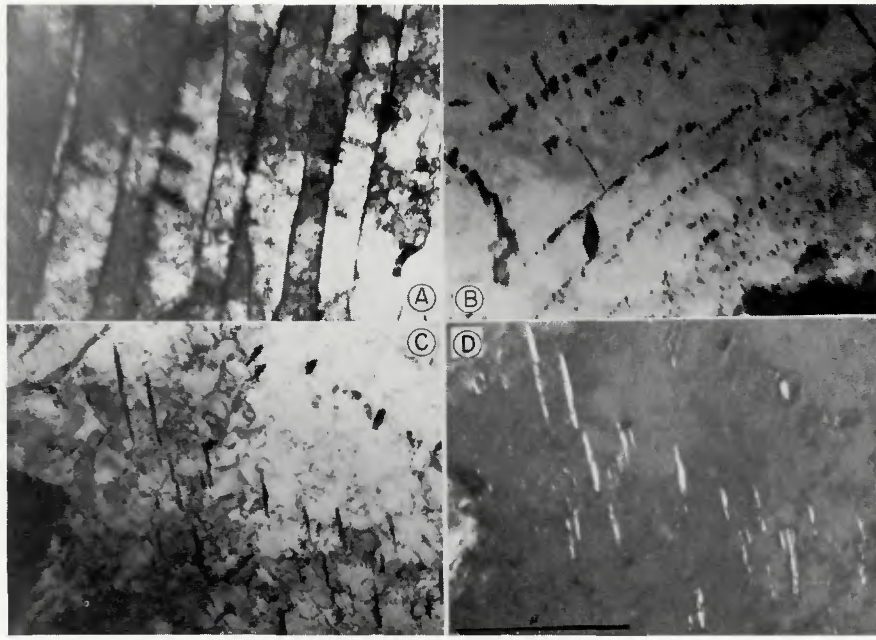

Fig. 6 — Microstructures of spot welded HF 50 steel after 50 Hz hold time: A — martensite laths intersecting undissolved cementite; B — carbides, both undissolved and reprecipitated; C — bright field image of reprecipitated cementite; D — dark field image of reprecipitated cementite

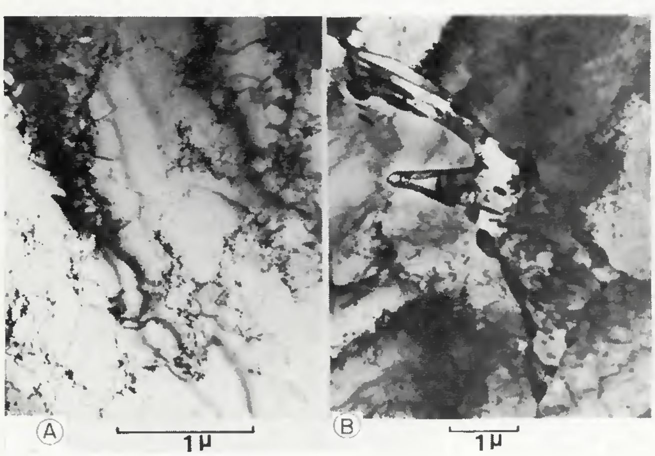

Fig. 4 — Base metal microstructures of HF 50 Cb-bearing steel: A — columbium carbonitride particles; B — degenerate pearlite structure

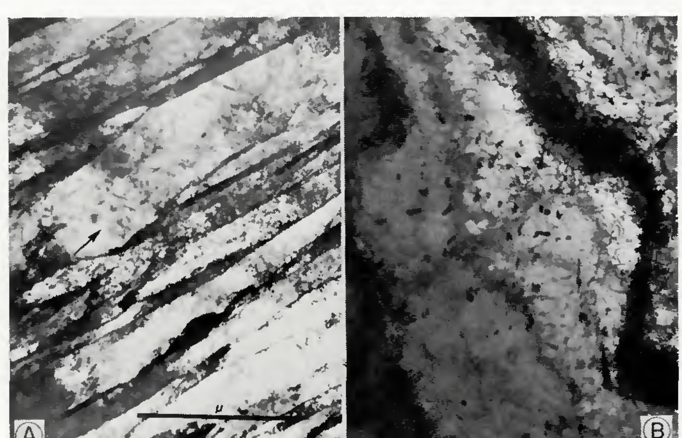

Fig. 5 — Microstructures of spot welded SAE 1005 steel after 50 Hz hold time showing: A — reprecipitated cementite in martensite lath; B — undissolved cementite in ferrite constitutent

observed in the specimen held for only 1 Hz after welding—Fig. 7A.

An arrow in Fig. 7A points to an area of very fine carbides. The carbides seem to be semi-coherent, because the surrounding matrix appears strained. Together with their morphology, this suggests that these carbides are reprecipitated columbium carbonitrides. In addition, the matrix microstructures appear more polygonal and massive with some sub-grains being formed. Undissolved carbides were also observed (not shown), but the plate-like carbides were less evident.

Hold time in resistance spot welding is the length of time the electrode is in contact with, and the electrode force is left applied on, the specimen after the passage of the weld current.* The electrode acts as a thermal sink to increase the cooling rate of the weld. This and the applied force induced the martensite formation which were observed in Figs. 5 and 6.

The martensitic structure with its higher dislocation density is the only factor that will explain the difference in the hardness profiles of the plain carbon steel after 50 and 1 Hz hold time. The shorter hold time means that the weld cooled much more slowly to produce the polygonal ferritic microstructure. The similarity of the hardness profiles of the specimens held for 50 Hz after welding indicates that the dominant microstructure contributing to the hardness is the martensite.

Although some columbium undoubtedly dissolved during welding, the fast cooling rate did not allow it to reprecipitate; thus, it must have contributed to hardenability. However, the hardness (strength) of martensite depends only on carbon content, and the hardness profiles reflect this. This explains the similarity in the profiles for the plain-carbon and columbium steels after the 50 Hz hold. In the slower cooled welds, the reprecipitation of columbium carbonitrides, which show some coherency strains, accounts for the higher hardnesses of the columbium steel.

*"Hold time" has been defined by the American Welding Society A2 Subcommittee on Definitions as the "duration of force application at the point of welding after the last impulse of current ceases."

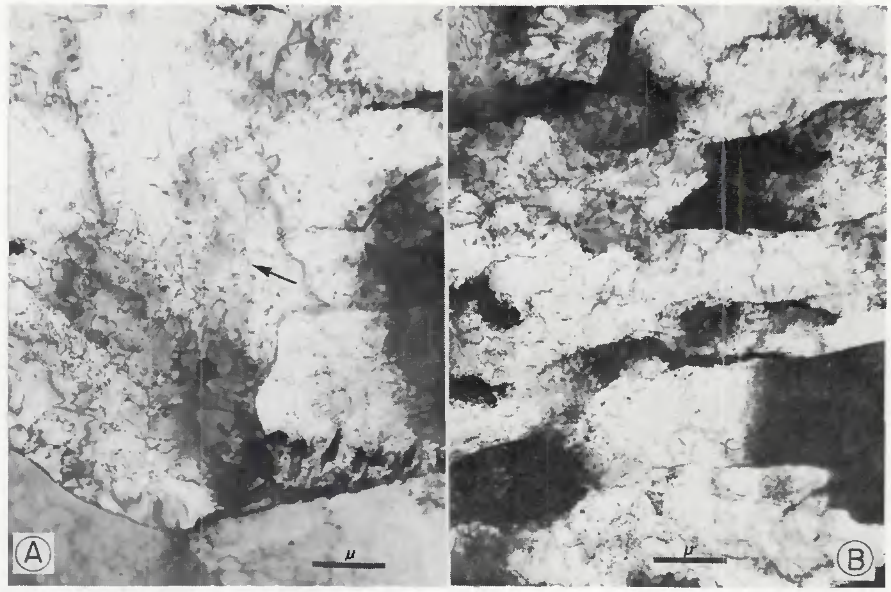

Fig. 7—Microstructures of spot welded HF 50 steel after 1 Hz hold time: A—arrow points to very fine Cb particles reprecipitated in polygonal ferrite; B—other typical ferritic structures

GMA Welding

The hardness profiles of the GMA welds are portrayed in Fig. 8. Considering Tables 4 and 5, the results show that alloy welding wire B and the lower input energy induced higher hardnesses in the weld than when the carbon steel welding wire A and higher input energies were employed. The use of alloy welding wire B and lower input energy induced more acicular structures. This can be discerned from Figs. 9 and 10, for the cases of alloy welding wire B and carbon steel welding wire A, respectively, used for mild steel.

The heat input for Fig. 9 and the acicularity in the structure is probably accounted for by the use of the alloy welding wire. It is also obvious that cementite did not completely dissolve during welding. Figure 9A represents areas where dissolution of cementite occurred, but the carbon concentration has not diffused sufficiently. In this case, the high carbon areas transformed to twinned martensite (T), while the low carbon areas transformed to either low carbon lath martensite (L) or massive ferrite.

When comparing the hardness profiles for the case where welding wire B was used, it is difficult to assess whether or not columbium has an effect. The reason for this is that the heat input for the plain carbon steel was considerably higher than that used for the Cb-bearing steel, *i.e.*, 5850 vs. 4550 J/in. (230.3 vs. 179.1 J/mm), Table 5. Undoubtedly, this affected the cooling rates of the welds; moreover, the lower heat input induced the faster cooling rate, which would induce more martensite. Any dissolved columbium would have also helped to produce more martensite to yield the higher hardness. When the heat inputs used were about the same, the weld hardnesses for both steels were about the same—Fig. 8. The higher heat-affected zone and base metal hardnesses for the columbium-bearing steel reflect the original properties in Table 2.

In addition to the microstructural differences demonstrated in Figs. 9 and 10, the columbium-bearing steel displayed changes in the columbium carbonitride precipitates with the changes in weld

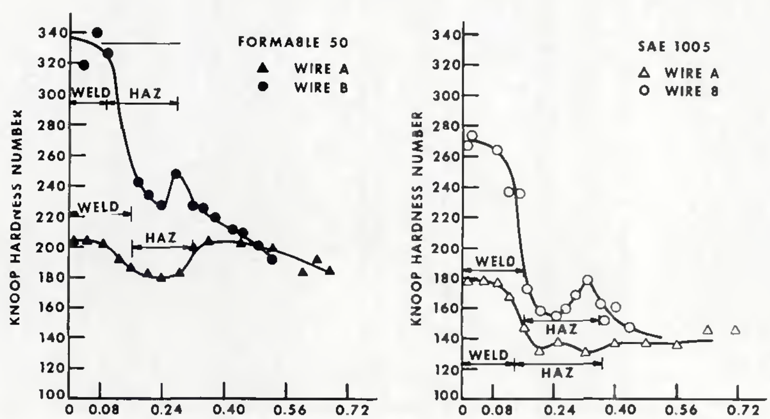

Fig. 8—Hardness profiles of GMA welds in HF 50 and SAE 1005 steels using conditions in Table 5; distances are in inches

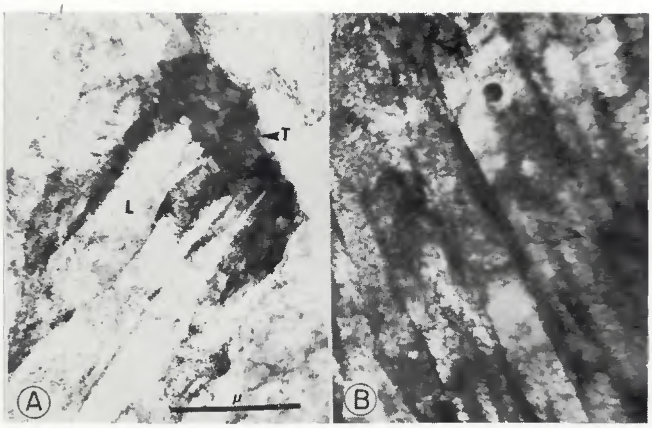

Fig. 9—HAZ structures of GMA-welded SAE 1005 steel using welding wire B and lower heat input: A—lath and twinned martensite structures indicating inhomogeneity in carbon; B—dislocated lath structures with undissolved cementite

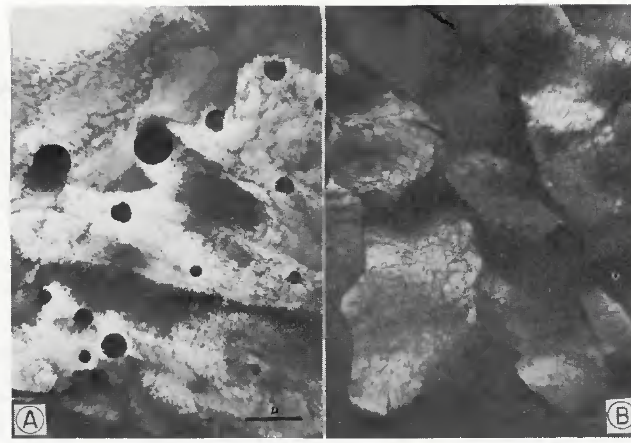

Fig. 10—HAZ structures of GMA-welded SAE 1005 steel using mild steel welding wire and higher heat input: A—large undissolved cementite; B—dislocations in polygonal ferrite

input energy. Figure 11 illustrates the effect of the lower weld heat input. The selected area diffraction (SAD) pattern pertains to Figs. 11A, B and C. Figure 11A is the bright field image from essentially a two-beam diffraction pattern and shows the typical mottled contrast of a strained matrix. There is no apparent large scale precipitation in this image but the diffraction pattern indicates otherwise because of the presence of extra spots. Indeed, when one of these spots was moved to the position of the transmitted beam and a dark-field image taken, fibrous-like precipitates were observed as shown in Fig. 11B.

The interplanar spacings from the extra spots in Fig. 11 match those from the ASTM index card for columbium nitride. However, because there is very little difference in the lattice parameters of the isomorphous columbium carbides and nitrides, it is safer to say these are columbium carbonitrides in the absence of a quantitative energy dispersive x-ray data.

The wavy nature of the fibrous-like precipitates suggests that they were formed at very high temperatures very close to their melting point. At this juncture, one recalls that eutectic linear carbonitrides were estimated to form at about 1350°C (2462°F) (Ref. 4) along grain boundaries. The carbonitrides in Fig. 11B are within the matrix and are considerably thinner than those reported (Ref. 4). It is conceivable that the precipitate morphology shown might be the precursor of the larger eutectic structures which form at the grain boundaries.

Figure 11C is the dark-field image of the strongest <110> spot in the diffraction pattern. Clearly, this image shows no semblance with Fig. 11B and is further evidence that the extra-spots in the inset diffraction pattern are independent of the matrix. Figure 11D is a bright-field image from another area showing heavy dislocation contrast. Careful examination of this image shows some evidence of the fibrous-like precipitates, but the dislocations masked the strain contrast seen in Fig. 11A.

With higher input energy, the morphology of the columbium bearing precipitate is as shown in Figs. 12A and 12D. The contrast shows very noticeable rosette-like features which are associated with particles. These features displayed ring-like diffraction patterns in the SAD, in addition to the $<100>_\alpha$ matrix spots. The ring-like pattern indicates random orientation of the precipitates.

Figure 12B is the dark-field image from a part of the ring pattern and shows the features to be an agglomeration of small particles. Separate small particles can be seen lighted up in the lower middle portion indicated by the arrow in Fig. 12B. The interplanar spacings from the ring-like patterns match those from $Cb_{(1-x)}S$ and some from MnS. Because of the inhomogeneous composition inherent in the short welding times, the precipitates might be a combination of $(MnCb)_xS$. Suffice to say, the columbium is associated with sulfur and possibly with nitrogen, as indicated earlier (Ref. 4).

The presence of a complex (Mn, Ti, Cb)S was observed in columbium-bearing steels in the vicinity of the fusion line (Ref. 2), and the sulfides were in the form of a two-dimensional eutectic film. The features seen in Figs. 12A (the bright

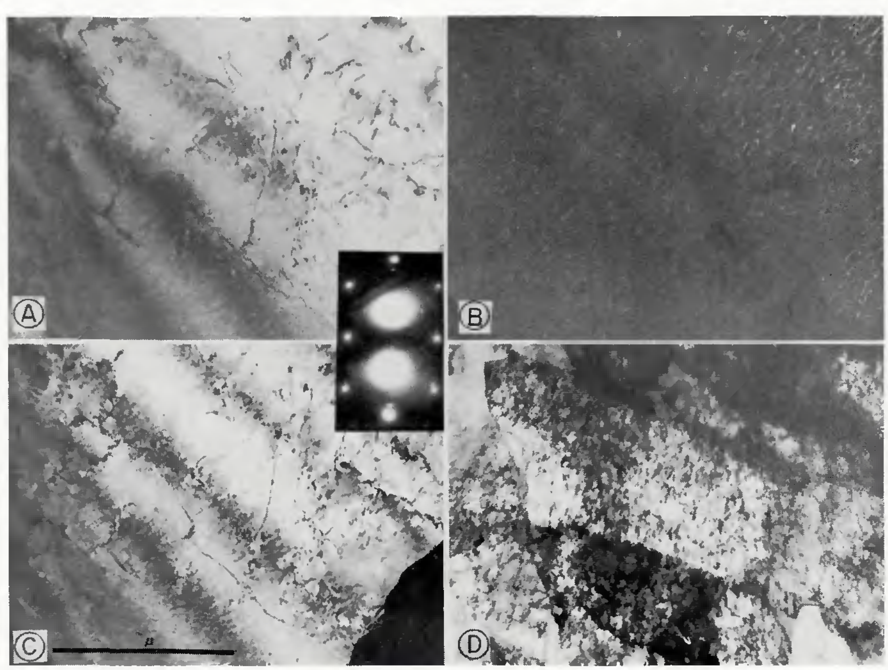

Fig. 11—HAZ microstructures of GMA-welded HF 50 steel using low heat input; inset diffraction pattern is primarily two-beam and shows extra precipitate spots: A—bright field image shows mottled contrast due to strained matrix; B—tilted dark field image of fibrous-like precipitate; C—tilted dark field image of matrix; D—bright field of another area

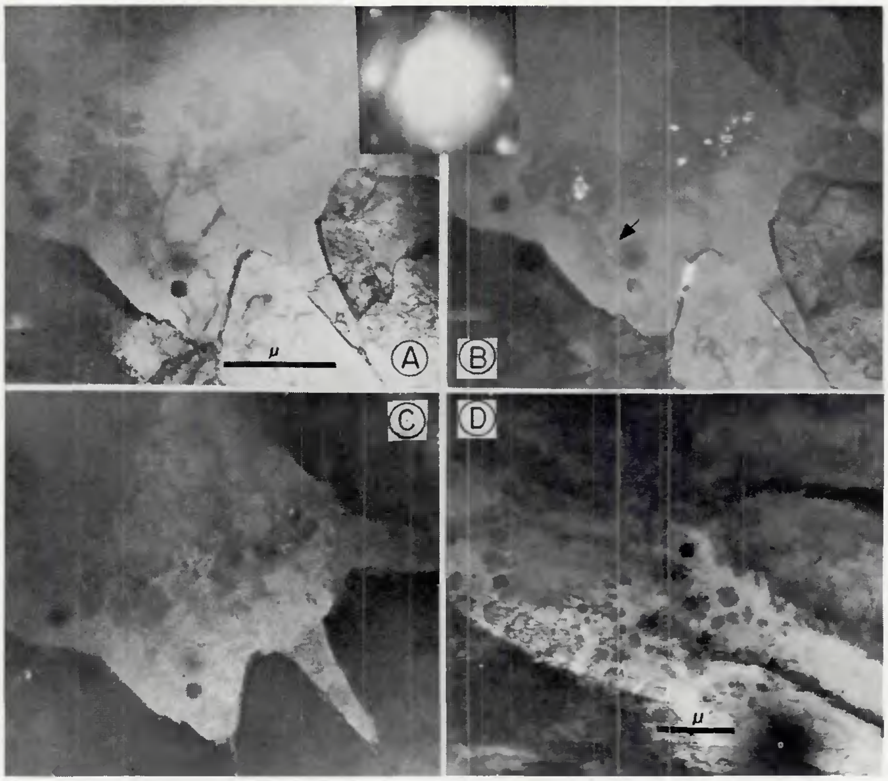

Fig. 12 — HAZ microstructures of GMA-welded HF 50 steel using the higher heat input; diffraction pattern is in <100> orientation with ring-like precipitate pattern: A — bright field showing rosette-like features; B — dark field from ring-like precipitate showing agglomeration of particles around rosette-like features (arrow points to isolated particles); C — bright field of matrix indicating penetration into neighboring grain as incipient melting; D — more rosette-like features and discernible particles associated with them

field), and 12C (the dark field ring of the matrix) suggest that this area underwent incipient melting of both matrix and precipitate. The matrix indicated by the dark-field image appeared to have melted, and the prior liquid was penetrating the grain-boundary in the lower right corner. This indicates that the temperature must have reached about 1500°C (2732°F) or more in this area.

As indicated earlier, the presence of the eutectic type nitrides, carbides, and sulfo-nitrides induced some hot-cracking and reduced ductility of the welds and heavy steel forgings and castings (Refs. 1-4). In the GMA welded specimens, the modifications of the columbium precipitates did not appear to impair the impact properties of the weld — Fig. 13 (Ref. 6). As shown in Fig. 13, the high-energy input-welded specimens exhibited a lower ductile brittle transition behavior. The results in Fig. 13 correlate well with the hardness profiles in Fig. 8 where the high-energy-input welds exhibited lower hardness (strength).

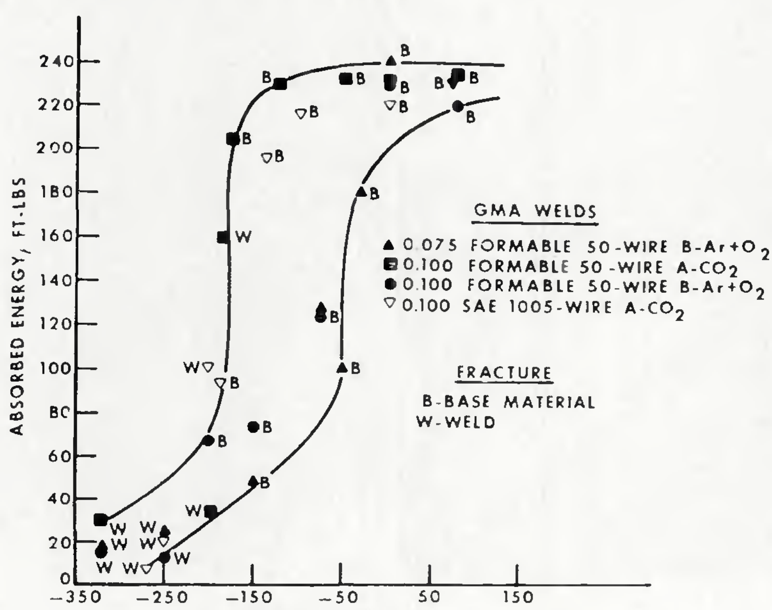

Fig. 13 — Ductile-to-brittle transition behavior of notched GMA welds in HF 50 and SAE 1005 steels using tension-impact specimens (Ref. 6)

The reason for the precipitates (described in this paper) not impairing the properties could be ascribed to their presence in the matrix and not in grain boundaries. This difference could be due to the much lower heat inputs used here in the GMA welded specimens compared to the submerged arc welding heat inputs, which usually range from 40 to 80 kJ/in. (1.6 to 3.1 kJ/mm). More study is needed — especially when very high energy inputs, *i.e.*, in excess of 100 kJ/in. (3.9 kJ/mm), are contemplated in submerged arc welding — to determine the nature of columbium precipitate modifications and their effects on the properties of the HAZ, the fusion line and the weld metal.

Conclusion

Transmission electron microscopy was conducted on thin foils of resistance spot- and GMA-welded columbium-microalloyed hot-rolled strip steel. For comparison, the structures of a similarly welded plain carbon steel were also examined. The following conclusions can be derived from this investigation:

1. In the short welding times employed, the carbides — both the cementite and the columbium carbonitride — do not completely dissolve. This results in local heterogeneities in composition in the weld and HAZ.

2. In resistance spot welding, long hold times (fast cooling rate) induce martensitic/acicular structures and prevent columbium carbonitrides from reprecipitation. In this case, the hardness profiles of both the plain carbon and the columbium-bearing steels were similar across the weld, and the martensitic structure is the dominant microconstituent. At shorter hold times (lower cooling rates), reprecipitation of Cb(CN) yielded higher hardnesses for the Cb-bearing steel.

3. In GMA welding, modifications in columbium precipitates were observed. Fibrous-like columbium carbonitrides were observed at the lower heat input used, and rosette-like features associated with agglomerated columbium particles were seen at the higher heat input welds. The observed modifications in columbi-

um did not impair the notch toughness. However, more study is needed to determine the influence of these modifications when much higher heat-inputs are used such as those in submerged arc welding.

Acknowledgment

This study was done under the employ of Inland Steel Company Research Laboratories. The author wishes to thank Inland Steel for permitting the results to be published.

The information provided by this paper was originally presented at a colloquium on micro-alloyed steels held November 23, 1983 at the Naval Research Laboratory and sponsored jointly by the Naval Research Laboratory and the David Taylor Naval Ship Research and Development Center.

References

1. Hrivnak, I. 1972. Metallurgical aspects of hot-crack formation in welded joints of micro-alloyed steels. *Zvaranie* 21 (4):104-108. BISITS 10485, Aug. 1973.

2. Hrivnak, I. 1971. Metallurgical aspects of the weldability of micro-alloyed steels. *Zvaranie* 20 (2):33-40. V. E. Riecansky Translation, VR/10/71.

3. Hannerz, N. E. *et al.* 1968. Brittleness in a cast steel caused by NbC precipitation. *J. Iron and Steel Inst.* 206: 68.

4. Hrivnak, I. 1973. Precipitation processes in converter steel micro-alloyed with niobium. *Kovove Materially* 11 (2):136-143. V. E. Riecansky Translation, VR/193/73.

5. Heitmann, W. E., Hilsen, R. R., Mangonon, P. L., and Moss, T. E. 1974. Development of a formable low carbon columbium bearing high strength hot-rolled sheet steel. SAE paper 740174, presented at the SAE Automotive Congress, Feb. 25-March 1, 1974, Detroit, Michigan.

6. Fostini, R. V., and Mangonon, P. L. 1974. Weldability of a formable low-carbon columbium bearing high-strength hot-rolled steel. Presented at the 13th Annual C.I.M. Conference, Aug. 25-28, 1974, Toronto, Canada.

7. Mangonon, P. L., and Heitmann, W. E. 1977. Sub-grain and precipitation-strengthening effects in hot-rolled, columbium-bearing steels. *Proceedings of micro-alloying 75,* p. 59. New York: Union Carbide Corporation.

Announcement and Call for Papers

The 3rd International Conference on Aluminum Weldments will be held at the Technical University of Munich, FRG, April 15–17, 1985. The Conference will cover all phases of aluminum weldments, including design and construction, applications, material characteristics and welding technology. The WRC Aluminum Alloys Committee is a cosponsor of the Conference. For more information, contact: W. W. Sanders, Jr., Engineering Research Institute, Iowa State University, 104 Marston Hall, Ames, Iowa 50011. (515)294-2336.

WRC Bulletin 296
July 1984

Fitness-for-Service Criteria for Pipeline Girth-Weld Quality
By R. P. Reed, M. B. Kasen, H. I. McHenry, C. M. Fortunko and D. T. Read

In this report, criteria have been developed for applying fitness-for-service analyses to flaws in the girth welds of the Alaska Natural Gas Transmission System pipeline. A critical crack-opening-displacement elastic-plastic fracture mechanics model was developed and experimentally modified. Procedures for constructing curves based on this model are provided. A significantly improved ultrasonic method for detecting and dimensioning significant weld flaws was also developed.

Publication of this report was co-sponsored by the National Bureau of Standards and the Weldability Committee of the Welding Research Council. The price of WRC Bulletin 296 is $16.50 per copy, plus $5.00 for postage and handling. Orders should be sent with payment to the Welding Research Council, Room 1301, 345 E. 47 St., New York, NY 10017.

Proceedings for the International Congress on Welding Research—July 13 and 14, 1984.

This Monograph contains the full texts for 9 papers and extended abstracts for 23 papers presented at the International Congress on Welding Research that was held just prior to the Annual Assembly of the International Institute of Welding, July 15–21, 1984, in Boston, Massachusetts. The theme of the Congress was "Welding Research in the World and the Challenges of the 80's" and was sponsored by IIW, WRC, AWS, WIC and ASM.

The price of the "Proceedings" is $25.00 per copy plus $5.00 for postage and handling. Orders should be sent with payment to the Welding Research Council, Room 1301, 345 E. 47 St., New York, NY 10017.

WRC Bulletin 299
November 1984

This bulletin contains three reports of work conducted under the guidance of the Subcommittee on Failure Modes in Pressure Vessel Materials of the Pressure Vessel Research Committee of the Welding Research Council. Funding for this three year project was supplied by the American Iron and Steel Institute and the Welding Research Council.

1. "Engineering Aspects of CTOD Fracture Toughness Testing," by G. W. Wellman and S. T. Rolfe. This report presents a study of the crack-tip opening displacement (CTOD) test method as a means of evaluating elastic-plastic fracture. Correlations with Charpy V-Notch, CTOD, J-integral, and stress intensity (K) notch-toughness parameters were investigated.
2. "Three-Dimensional Elastic Plastic Finite-Element Analysis of Three-Point Bend Specimens," by G. W. Wellman, S. T. Rolfe and R. H. Dodds.

   This report summarizes the verification of analytical procedures for use in flawed structures. As a first step toward analyzing the more complex structures of a pressure vessel, the three-point bend specimen was analyzed using both 2-D and 3-D elastic-plastic finite-element analysis methods. CTOD and J values determined from these analyses were compared to the experimental results of the five steels investigated in the first paper.
3. "Failure Prediction of Notched Pressure Vessels Using the CTOD Approach," by G. W. Wellman, S. T. Rolfe and R. H. Dodds.

   This report analyzes the behavior of five notched pressure vessels tested at temperatures such that the failure mode varied from fully ductile to brittle behavior. Both 2-D and 3-D finite-element analyses were used to analytically develop curves of pressure versus opening of the flaw in the vessel. The internal pressures corresponding to the minimum CTOD values obtained from the vessel steels were within 7% of the actual burst pressures.

The results of these works contribute significantly to the understanding and predicting of the different failure modes that can occur in pressure-vessel steels.

The price of WRC Bulletin 299 is $13.50 per copy, plus $5.00 for postage and handling. Orders should be sent with payment to the Welding Research Council, Rm. 1301, 345 E. 47 St., New York, NY 10017.

WRC Bulletin 294
May 1984

Creep of Bolted Flanged Connections
by H. Kraus and W. Rosenkrans

In this report, a previous analysis of the creep of bolted flanged connections by E. O. Waters is extended to include strain hardening creep and an unspecified distribution of stress over the flange rings. The results are compared to a finite element analysis and to results obtained with Waters' equations.

Short Term Creep and Relaxation Behavior of Gaskets
by A. Bazergui

This report presents the results of short term creep tests at constant stress levels, cyclic creep tests, and relaxation tests for four types of gaskets.

Publication of this bulletin was sponsored by the Subcommittee on Bolted Flanged Connections of the Pressure Vessel Research Committee of the Welding Research Council. The price of WRC Bulletin 294 is $12.75 per copy plus $5.00 for postage and handling. Orders should be sent with payment to the Welding Research Council, Room 1301, 345 E. 47th St., New York, NY 10017.

AWS "Peer Review" Panel

The individuals whose names are listed below are participating in the "Peer Review" Program of the American Welding Society as it pertains to the Research Supplement of the *Welding Journal*. Participation consists of evaluating the technical content of papers submitted for publication in the Research Supplement and, to this end, rendering judgments concerning:

- Originality of the contribution.
- Technical value to the welding community.
- Prior publication of the material being reviewed.
- Proper credit to others working in the same technical area.
- Justification of the conclusions judging by the results.
- Degree of acceptability for publication.

It is considered that program participants are rendering an invaluable service to the welding community and to the authors of papers undergoing review. Others wishing to serve as reviewers are asked to contact the Technical Editor of the *Welding Journal*, P.O. Box 351040, Miami, FL 33135.

Current Reviewers

D. K. Aidun
G. A. Andreano
W. R. Apblett Jr.
D. G. Atteridge
W. G. Bader
W. A. Baeslack, III
J. C. Baker
D. J. Ball
C. M. Banas
R. E. Beal
F. Beaver
L. S. Beedle
C. R. Behringer
R. Beldyk
W. P. Benter, Jr.
J. T. Biskup
W. Borges
K. L. Brown
A. J. Bryhan
J. M. Cameron
D. A. Canonico
R. S. Chandel
D. U. Chang
R. A. Chihoski
M. Cieslak
N. S. Cole
C. E. Cross
S. A. David
R. DeNale
P. B. Dickerson
D. W. Dickinson
R. D. Dixon
R. B. Dooley
R. J. Dybas
T. W. Eagar
B. J. Eberhard
D. P. Edmonds
G. Edwards
J. W. Elmer
J. W. Fisher
E. A. Flynn
W. R. Frick
E. Friedman
L. M. Friedman
E. B. Gempler
J. M. Gerken
F. E. Gibbs
S. S. Glickstein
G. M. Goodwin
F. J. Grist
J. R. Hannahs
D. W. Harvey
D. C. Helton
R. T. Hemzacek
D. E. Hetzel
G. K. Hicken
T. Hikado
J. F. Hinrichs
D. G. Howden
E. I. Husa
J. E. Indacochea
C. E. Jackson
J. J. Jellison
J. E. Jones
P. A. Kammer
W. A. Kawahara
J. F. Key
R. A. Kelsey
J. F. King
W. H. King
G. A. Knorovsky
P. J. Konkol
L. J. Korb
D. J. Kotecki
S. Kou
J. S. Kozelski
F. V. Lawrence, Jr.
G. L. Leone
G. G. Lessmann
D. Link
J. C. Lippold
R. E. Long
C. R. Loper, Jr.
C. D. Lundin
K. A. Lyttle
A. F. Manz
R. P. Martukanitz
K. Masubuchi
D. K. Matlock
S. J. Matthews
R. B. McCauley
J. T. McGrath
H. I. McHenry
E. A. Metzbower
G. E. Metzger
J. A. Miller
J. W. Mitchell
A. J. Moorhead
W. H. Munse
T. M. Mustaleski
T. V. Natale
C. D. Nicky
E. F. Nippes
T. H. North
D. L. Olson
G. W. Oyler
V. J. Papazoglou
B. M. Patchett
D. W. Patterson
R. A. Patterson
A. W. Pense
D. D. Peter
E. Pfender
L. E. Pope
M. Prager
D. D. Rager
K. B. Rao
D. T. Read
W. S. Ricci
R. W. Richardson
G. D. Ries
A. M. Ritter
I. B. Robinson
M. N. Ruoff
E. P. Sadowski
W. W. Sanders, Jr.
L. W. Sandor
S. J. Santangelo
W. F. Savage
J. M. Sawhill, Jr.
M. M. Schwartz
E. G. Shifrin
L. E. Shoemaker
T. A. Siewert
G. M. Slaughter
J. P. Snyder, II
R. E. Somers
D. E. Spindler
J. Spingarn
G. R. Stoeckinger
R. D. Stout
M. A. Streicher
R. D. Sutton
J. R. Terrill
R. D. Thomas, Jr.
C. L. Tsai
A. J. Turner
G. D. Uttrachi
J. J. Vagi
T. L. VanderWert
R. Vasudevan
S. Venkataraman
R. C. Voigt
F. A. Wassell
T. A. Whipple
W. L. Wilcox
W. L. Winterbottom
C. E. Witherell
J. R. Woodward
K. C. Wu
H. Y. Yoon
C. A. Zanis